Disclosing the magnetic ground state of $PrBaMn_2O_6$.

J. Blasco,[1,a)] J. A. Rodríguez-Velamazán,[1,2] J. L. García-Muñoz,[3] and G. Subías.[1]

[1]*Instituto de Nanociencia y Materiales de Aragón, Dep. Física de la Materia Condensada, CSIC-Universidad de Zaragoza, 50009 Zaragoza , Spain*

[2]*Institute Laue Langevin, BP 156, 38042 Grenoble Cedex 9, France*

[3] *Institut de Ciència de Materials de Barcelona, ICMAB-CSIC, Campus univ. de Bellaterra, E-08193 Bellaterra, Spain*

We here report a neutron diffraction study on a single crystal of the layered $PrBaMn_2O_6$ perovskite. This compound undergoes two consecutive magnetic transitions with decreasing temperature. At $T_C \approx 309$ K, a long-range ferromagnetic ordering is established with the Mn magnetic moments oriented along the *c*-axis. Below $T_N \approx 240$ K, a spin reorientation gives rise to a sudden decrease of the magnetization and the formation of an antiferromagnetic order. This magnetic transition is also accompanied by an electronic localization caused by a structural phase transition from a high temperature tetragonal phase (*P4/mmm*) into a low temperature orthorhombic one ($P2_1am$). Our neutron diffraction study at 12 K has unambiguously identified that the ground magnetic structure for this compound is a layered antiferromagnetic structure along the c-axis with the Mn moments oriented in the *ab*-plane along one diagonal of the primitive tetragonal cell. No sign of magnetic scattering associated to a CE-type magnetic structure was found in our study, discarding its occurrence in this compound. This result excludes the occurrence of a charge order transition to account for the electronic localization and it is fully consistent with previous structural studies showing a unique crystallographic site for Mn atom in the low temperature phase. A symmetry analysis was carried out to identify the magnetic space group of the ferromagnetic order above T_N and the two possible groups for the antiferromagnetic ordering below T_N.

[a)] Author to whom correspondence should be addressed. Electronic mail: jbc@unizar.es

1. INTRODUCTION.

Mixed oxides of Mn and rare earth, the so-called manganites, have been widely studied for the last 20 years due to their interesting applications such as giant magnetoresistance for electronic devices, and their exciting physical properties arising from the competition between electronic, charge, magnetic, and orbital degrees of freedom [1-4]. These competitive forces are enhanced in half-doped manganites giving rise to new exotic phases [5,6]. Manganites adopt either the ABO_3 perovskite structure or derivatives (such as Ruddlesden-Popper phases). At first it was thought that the large cations that occupy the A-position had the only function of stabilizing the crystal structure, and the B-O-B (Mn-O-Mn) interactions were responsible for the observed physical properties. However, recent studies have revealed that an ordered arrangement of A-atoms has a great influence on the properties of half-doped manganites respect to compounds where A-atoms are randomly distributed [7].

This is the case for $RBaMn_2O_6$ compounds where R (Rare earth or Y) and Ba atoms are ordered in layers along the *c*-axis. The undistorted crystal structure for $RBaMn_2O_6$ is tetragonal in contrast with the primitive cubic cell of disordered $R_{1/2}Ba_{1/2}MnO_3$ compounds (see Fig. 1). Due to the different size of R and Ba atoms, asymmetric distortions are forced in the MnO_6 octahedra, as can be seen in the Fig. 1 [7,8]. These forced distortions give rise to different physical properties compared to their disordered counterparts, $R_{1/2}Ba_{1/2}MnO_3$ [7,9,10,11], which depend on the R cation size. Overall, magnetic interactions and charge localization processes are enhanced in the ordered perovskites. For the case of the largest R-atom (La), the layered A-site order enhances the ferromagnetic (FM) interaction. Thus, both $La_{1/2}Ba_{1/2}MnO_3$ and $LaBaMn_2O_6$ have a FM ground state but the Curie temperature (Tc) is about 50 K higher in the ordered sample [9,11]. The change is more drastic for smaller R-atoms (R=Sm, Eu, Gd, Tb or Y for instance). The disordered samples do not present long-range magnetic order but magnetic glassy properties [10,11]. However, the samples with the layered A-site order develop a CE-type antiferromagnetic (AFM) order [12] with Neel temperatures (T_N) close to 200 K. In addition, these compounds present structural transitions well above T_N associated to charge order (CO) transitions [11]. These CO phases appear at higher temperatures as the R-cation size decreases, and different CO patterns have been reported depending on the R-type [13-16]. Moreover, the CO phases are absent in the disordered samples [7,9]. For R-sizes intermediate between the two previous groups (Pr or Nd) the situation is a little more complicated. The disordered samples present glassy magnetic properties although with higher transition temperatures, typical of the presence of short-range FM clusters [8,9,11]. However, in the ordered samples competitive magnetic interactions of different sign are observed. Two magnetic transitions are noticeable in $PrBaMn_2O_6$ where a FM transition at T_C = 309 K is followed by an AFM order at $T_N \approx$ 240 K on cooling [17,18]. T_N and T_C approach each other so closely in $NdBaMn_2O_6$ that the magnetization curves resemble that of a weak FM and there is controversy over whether a true long-range FM order is established before AFM order occurs ($T_N \approx$ 285 K) in this compound [19,20]. In Pr and Nd compounds, the AFM transition is coupled to both a structural phase transition and a metal-insulator-like transition that resembles a CO transition in related simple manganites [18, 21]. The nature of this transition has been subject of debate. A model based on a ferroic orbital order of $Mn^{3.5+}$ *3d*-orbitals was developed by Yamada *et al.* to explain the metal-insulator-like transition in these compounds [21] in

absence of CO. Later, some of the previous authors performed a subsequent X-ray study on a single crystal of $NdBaMn_2O_6$ using synchrotron radiation [22]. Their results suggested that this compound was isostructural to $SmBaMn_2O_6$ and therefore the metal-insulator transition was associated with a CO transition as opposed to the ferroic orbital model [21]. The ferroic orbital model, however, is more compatible with our recent structural studies of the Pr and Nd compounds based on X-ray powder diffraction using synchrotron radiation [18]. It was observed that the low temperature phase of these two compounds adopts an orthorhombic cell with a single crystallographic site for Mn atoms, which prevents a CO pattern [18]. Furthermore, a very recent EXAFS study confirms the occurrence of a tiny local distortion of the MnO_6 octahedra below T_N [11], characteristic of a charge-localized phase, but without a significant charge segregation in agreement with the crystallographic studies showing a single site for the Mn atom in the low-temperature polar structure. Finally, layered manganites with a CO transition present a CE-type AFM order while early neutron powder diffraction studies established an A-type AFM order for the $NdBaMn_2O_6$ compound and a mixture of CE- and A-types magnetic orderings for $PrBaMn_2O_6$ [19].

In order to shed light on the previous controversies, it is essential to determine the magnetic ground state of $PrBaMn_2O_6$ and for that purpose we have carried out a neutron diffraction study on a quality single crystal of this compound. We have clearly identified that this compound undergoes a FM transition at high temperature and, on cooling, a spin reorientation leads to a single AFM phase. We have determined the direction of the magnetic moments in both magnetic orderings and a symmetry analysis have allowed us to identify the magnetic space groups adopted by $PrBaMn_2O_6$ in its two magnetic regimes.

2. EXPERIMENTAL SECTION.

Single crystals of $PrBaMn_2O_6$ were grown using the floating zone method from polycrystalline precursors as indicated elsewhere [18]. Stoichiometric amounts of dried Pr_6O_{11}, $BaCO_3$ and Mn_2O_3 were mixed, ground and heated at 1000ºC overnight. The resulting powder was reground, pressed into pellets and sintered at 1250ºC in a gas flow of H_2/Ar mixture (2 % of H_2) saturated in water vapor to achieve a reductive atmosphere ($P_{O2} \approx 10^{-11}$). This is required to prevent the formation of $BaMnO_3$ impurity [23]. Then, the pellets were reground, pressed into rods and sintered at 1325ºC for 24h in the same atmosphere. The rods were mounted in a homemade floating zone furnace with two semi-elliptical mirrors [24,25]. The growth was performed in the same reductive atmosphere with an overpressure of 2 bars. The seed and feed bars with diameters of 3.5 mm rotated in opposite directions at 20 rpm with a growth speed of 6 mm/h. Parts of the boules were cleaved to yield shiny and flat [0 0 1] faces. The resulting compounds have an oxygen-deficient stoichiometry, $PrBaMn_2O_{5+\delta}$ ($\delta \approx 0.1$) as reported for $SmBaMn_2O_{5+\delta}$ [25]. In order to obtain the desired stoichiometry, a topotactic oxidation was carried on. The boules were oxidized in an oxygen current flow at 400ºC for 1 day. Some pieces were ground and analyzed by powder X-ray diffraction at room temperature using a Rigaku D-Max system and Cu K_α radiation. The pattern was consistent with a single phase $PrBaMn_2O_6$ compound [18]. The chemical composition of the specimens was also tested using wavelength dispersive X-ray fluorescence spectrometry (Advant'XP+ model from

Thermo-Fisher) and the Pr:Ba:Mn stoichiometry agreed with the expected values within the experimental error (1%).

Single-crystal neutron diffraction data were collected on the high resolution four-circle diffractometer D9 at the ILL (Grenoble, France) using the wavelength of 0.832(1) Å obtained by reflection from a Cu (220) monochromator. The wavelength was calibrated using a single crystal of Ge. A small two-dimensional (2D) area detector of 6 × 6 cm (32 × 32 pixels) allows reciprocal space survey and optimization of the peak position. The program RACER [26] was used to integrate the omega- and omega-2theta-scans and to correct them for the Lorentz factor. The crystal attenuation corrections were performed with a prism model using DATAP program, [27]. Fullprof package program [28] was used for the analysis of single-crystal neutron diffraction data. The schematic illustrations of the crystal structures were obtained with the VESTA program [29]. Crystallographic tools from the Bilbao Crystallographic Server [30] and the ISOTROPY software suite [31] were also used to perform the symmetry analysis.

Magnetic measurements on powder samples were carried out between 5 and 400 K by using a commercial superconducting quantum interference device (SQUID) and a Physical Properties Measuring System (PPMS) from Quantum Design. The measurements were performed warming the sample after zero-field cooling at an external magnetic field of 1 kOe and then cooling in the same field. Isothermal magnetization measurements at 5 and 283 K (heating run) were performed for externals fields between -50 and 50 kOe.

3. RESULTS AND DISCUSSION.

A single crystal with a flake shape and a shiny face corresponding to the (0 0 1) reflection was used. The collection of reflections at room temperature agrees with a tetragonal lattice (a=3.889(1) Å; c= 7.7317(2) Å) with space group *I4/mmm* as previously reported [18]. Figure 2 compares the temperature dependence of the magnetization for $PrBaMn_2O_6$ with the intensity of selected reflections. As reported previously [8,18,19], this compound undergoes two consecutive phase transitions. The FM transition has T_C=309 K calculated from the inflection point of the M(T) curve. Below this temperature, this compound undergoes an AFM transition whose T_N strongly depends on the scan conditions (cooling or heating) due to a noticeable hysteresis of about 25 K [18]. At T_N, $PrBaMn_2O_6$ undergoes a structural phase transition adopting a polar orthorhombic structure with space group $P2_1am$ [18]. The relationships between the high temperature tetragonal phase and the low temperature orthorhombic one are $a_O = \sqrt{2}\, a_T$, $b_O = \sqrt{2}\, b_T$ and $c_O = c_T$ where O and T subscripts refer to the orthorhombic and tetragonal unit cells, respectively. With decreasing temperature, the main magnetic contribution is observed in the $(even, even, odd)_O$ reflections as can be seen in the Fig. 2(a). The onset of this magnetic contribution coincides with T_N in the M(T) curve marked by a strong drop in the magnetization value. These magnetic reflections are typical of an A-type AFM ordering [12] corresponding to a magnetic propagation vector $\boldsymbol{k}$=0 respect to the low temperature orthorhombic phase. In order to verify if this is the only magnetic phase present in this compound, scans were made in the reciprocal space (Q-scans) at 12 K looking especially for reflections that followed the propagation vector $\boldsymbol{k}$= $(½\ ½\ ½)_T$ characteristic of a CE-type order [19]. No

reflections were observed to suggest that the *c*-axis is doubled. This ruled out the existence of a CE-type magnetic contribution in this compound. What we did observe were reflections following the propagation vector $\boldsymbol{k}$= (½ ½ 0)$_T$ corresponding to the abovementioned structural phase transition. We followed the intensity of the (½ ½ 1)$_T$ reflection in a heating run (see Fig. 2(b)) and it vanishes around T_N revealing the coupling between the magnetic and the structural phase transitions. We also followed the nuclear (1 1 0)$_T$ reflection on heating (see Fig. 2(b)). It shows a local maximum at around 283 K (between T_N and T_C) disclosing the maximum FM contribution in this sample on the heating ramp. Figure 3 compares the isothermal magnetization curves measured at 5 and at 283 K. The measurement at 5 K shows a linear behavior characteristic of the lack of spontaneous magnetization (*i.e.*, paramagnetic or AFM behavior). Instead, a clear hysteresis loop is noticeable in the measurement at 283 K. In addition to the spontaneous magnetization, a linear behavior is observed in the loops at high magnetic fields and magnetic saturation, whose expected value is 7 μ_B/*f.u.*, is not achieved at 50 kOe. Therefore, $PrBaMn_2O_6$ is not fully polarized at this temperature.

According to these results we selected two temperatures, 12 and 283 K, to perform a neutron data collection to determine the two magnetic structures inferred for this compound. We also made a neutron data collection at 320 K in order to characterize the paramagnetic phase. Direct comparison of the intensities measured at 320 and 283 K clearly indicates an increase in the intensity of some reflections perpendicular to the *c*-axis (see Fig. 2(b)) suggesting that the Mn moments are aligned along this axis. Symmetry analysis was performed using tools from the Bilbao Crystallographic Server [30] and the ISOTROPY software suite [31]. The search of magnetic structures with $\boldsymbol{k}$=0 that preserve the tetragonal unit cell [18] only yields two results and the only one permitting a FM alignment of Mn moments corresponds to the magnetic space group *P4/mm'm'* (No. 123.345 in BNS notation [32]), with the FM ordering of Mn moments being along the *c*-axis, in agreement with the experimental results. The ferromagnetic structure transforms as the magnetic irreducible representation (mirrep) mΓ_3^+. We used this model to refine the neutron data at 283 K obtaining an accurate fit as can be observed in the Figure 4. The refined Mn moment at that temperature was 1.51(2) μ_B/Mn, quite below the one expected for full polarized Mn sublattice with a formal +3.5 valence (3.5 μ_B/Mn). The lack of full polarization agrees with the isothermal measurement (see Fig. 3). Fig. 4 also shows the FM structure of $PrBaMn_2O_6$ and further details of this magnetic structure are summarized in the Table 1.

The neutron data at 12 K was analyzed using the low temperature phase orthorhombic cell. The evolution of the magnetic peaks clearly reveals that magnetic moments are mainly placed perpendicular to the *c*-axis (see Fig. 2). The search of magnetic structures of the $P2_1am$ crystal structure with $\boldsymbol{k}$=0 using the Isodistort tool yields four possibilities but only two of them are compatible with an A-type ordering perpendicular to the *c*-axis. They correspond to the magnetic space groups $P2_1am$ (No. 26.66) and $P2_1'a'm$ (No. 26.69), both with transformation to the standard setting (**-c**,**b**,**a**;0,0,0). According to Bertaut's notation [33], the resulting magnetic structures would be $G_xA_yC_z$ ($P2_1am$) and $A_xG_yF_z$ ($P2_1'a'm$). The occurrence of forbidden nuclear reflections for $P2_1am$ space group revealed that our crystal was twinned at low temperature with an even mixture of two domains, namely *abc* and *ba-c*. In this way, the forbidden reflection (*odd, 0, l*) in one

domain is allowed in the other one as (*0, odd, -l*). This fact prevents to discern between the two previous magnetic models. Both models, or a combination of them, allow good fits of the experimental data although the combination is very unlikely as it implies the combination of two different mirreps. In any case, only one component is enough to refine the neutron data and we have not detected any magnetic contribution ascribed to F- or C-type contributions. Therefore, in a magnetic domain the Mn moments are collinearly aligned along one of the crystallographic axes in the *ab*-plane of the low temperature orthorhombic phase (or equivalently along one diagonal in the *ab*-plane of the high temperature tetragonal phase). The definitive direction (m_y in $P2_1am$ or m_x in $P2_1'a'm$) could only be obtained by analyzing an untwinned single crystal at low temperature, which could be very challenging due to the tetragonal-orthorhombic phase transition concurrent at T_N (see Fig. 2(b)). Figure 5 shows the best fit obtained with the second magnetic structure, $A_xG_yF_z$ ($P2_1'a'm$ (**-c**,**b**,**a**;0,0,0)), which exhibits somewhat better reliability factors. The corresponding magnetic structure is also displayed in Fig. 5 and the refined parameters are summarized in the Table 2. The refined Mn moment was m_x=3.11(2) μ_B/Mn, close to the one expected for the mixed valence Mn. This solution is particularly attractive because, by symmetry, it allows a FM component in the *z*-direction as occurs in the FM order of the tetragonal phase above T_N. Furthermore, if this component could be induced through some doping, it would be a way to obtain new magnetoelectric multiferroic compounds because the $P2_1am$ space group allows ferroelectric order along the *a*-axis.

In general, our study is in agreement with previous results obtained using neutron powder diffraction [19]. A similar A-type ordering was deduced for both $NdBaMn_2O_6$ and $PrBaMn_2O_6$. However, a minor CE-type contribution was observed in the pattern of the polycrystalline $PrBaMn_2O_6$ compound undetected in our single crystal. We believe that this discrepancy reflects that the polycrystalline sample studied in ref. 19 was not optimized and presented some small impurity (traces of simple perovskite and/or different Pr:Ba stoichiometry) responsible for the small CE-type peaks.

4. CONCLUSIONS.

The magnetic ground state of $PrBaMn_2O_6$ has been proved by means of single crystal neutron diffraction. Below $T_N \approx 240$ K, this manganite adopts an A-type AFM ordering with the Mn moments aligned along one crystallographic axis in the *ab*-plane of the low temperature orthorhombic phase. The possible magnetic space groups have been circumscribed (either $P2_1am$ or $P2_1'a'm$). There is no sign of a CE-type AFM order in this compound and this result has important consequences on the physical properties of $PrBaMn_2O_6$. In particular, the metal-insulator-like transition coupled to the tetragonal-orthorhombic phase transition cannot be ascribed to a CO phase transition as occurs in $SmBaMn_2O_6$ [22] but to a condensation of phonons [18] that opens a gap in the conduction band, similar to $NdBaMn_2O_6$ [11] and thus may be related to the establishment of a ferroic orbital order [21]. In addition, we have verified that a long-range FM order develops in this compound above T_N, without achieving full moment polarization. The Mn moments are collinearly coupled along the *c*-axis and the magnetic space group has been identified as *P4/mm'm'*.

Acknowledgements.

The fruitful discussions and long years of collaborations with Prof. Juan Bartolomé are truly appreciated by the authors.

For financial support, we thank grants PID2021-124734OB-C21 and RTI2018-098537-B-C22 funded by MCIN/AEI/10.13039/501100011033 and, as appropriate, by "ERDF A way of making Europe", and "Severo Ochoa" Programme for Centres of Excellence in R&D (CEX2023-001282-S and CEX2023-001263-S); and Gobierno de Aragón (Project E12-23R). Granted beam time at ILL is also appreciated (Experiment No. 5–41–1121). Authors would also like to acknowledge Servicio General de Apoyo a la Investigación from Universidad de Zaragoza.

References.

[1] E. Dagotto, T. Hotta, and A. Moreo, Phys. Rep. **344**, 1 (2001).

[2] Y. Tokura, Rep. Prog. Phys. **69**, 797 (2006).

[3] G. Subías, J. García, J. Blasco, and M. G. Proietti. Phys. Rev. B **57**, 748 (1998).

[4] S. Li, Z. X. Lu, B. Lao, X. Zheng, G. X. Chen, R. W. Li, Z. M. Wang, Appl. Phys. Lett. **124**, 172403 (2024).

[5] Y. Tokura and N. Nagaosa, Science **288**, 462 (2000).

[6] J. Blasco, V. Cuartero, S. Lafuerza, J. L. García-Muñoz, F. Fauth and G. Subías, Phys. Rev. B **109**, 024111 (2024).

[7] Y. Ueda and T. Nakajima, Prog. Solid State Chem. **35**, 397 (2007).

[8] T. Nakajima, H. Kageyama, H. Yoshizawa, and Y. Ueda, J. Phys. Soc. Jpn. **71**, 2843 (2002).

[9] T. Nakajima, and Y.Ueda, J. Allows and Comp. **383**, 135 (2004)

[10] T. Nakajima, H. Yoshizawa, and Y. Ueda, J. Phys. Soc. Jpn. **73**, 2283 (2004).

[11] G. Subías, J. Blasco, V. Cuartero, S. Lafuerza, L. Simonelli, G. Gorni , M. Castro, and J. García, Phys. Rev. B **107**, 165133 (2023).

[12] E. O. Wollan and W. C. Khoeler, Phys. Rev. **100**, 545 (1955).

[13] A. J. Williams, J. P. Attfield, S. A. T. Redfern, Phys. Rev. B **72**, 184426 (2005).

[14] J. Blasco, G. Subías, J. L. García Muñoz, F. Fauth, M. C. Sánchez, and J. García, Phys. Rev. B **103**, 214110 (2021).

[15] H. Sagayama, S. Toyoda, K. Sugimoto, Y. Maeda, S. Yamada, and T. Arima, Phys. Rev. B 90, 241113(R) (2014).

[16] J. Blasco, G. Subías, J. L. García Muñoz, F. Fauth, and J. García, Joaquín J. Phys. Chem C **125**, 19467 (2021).

[17] H. Kageyama, T. Nakajima, M. Ichira, Y. Ueda, H. Yoshizawa, and K. Ohoyama,. J. Phys. Soc. Jpn. **72**, 241 (2003).

[18] J. Blasco, G. Subías, M. L. Sanjuán, J. L. García-Muñoz, F. Fauth, and J. García, Phys. Rev. B **103**, 064105 (2021).

[19] T. Nakajima, H. Kageyama, H. Yoshizawa, K. Ohoyama, and Y. Ueda, J. Phys. Soc. Jpn. **72**, 3237 (2003).

[20] D. Akahoshi, Y. Okimoto, M. Kubota, R. Kumai, T. Arima, Y. Tomioka, and Y. Tokura, Phys. Rev. B **70**, 064418 (2004).

[21] S. Yamada, H. Sagayama, K. Higuchi, T. Sasaki, K. Sugimoto, and T. Arima, Phys. Rev. B **95**, 035101 (2017).

[22] S. Yamada, N. Abe, H. Sagayama, K. Ogawa, T. Yamagami, and T. Arima, Phys. Rev. Lett. 123, 126602 (2019).

[23] F. Millange, V. Caignaert, B. Domengès, B. Raveau, and E. Suard, Chem. Mater. **10**, 1974 (1998).

[24] J. Blasco, M. C. Sánchez, J. García, J. Stankiewicz, and J. Herrero-Martín, J. Cryst. Growth **310**, 3247 (2008).

[25] J.Blasco, J.A. Rodríguez-Velamazán, G. Subías, M.C. Sánchez, and J. L. García-Muñoz, Mat. Res. Bull. **150**, 111780 (2022).

[26] M. S. Lehmann, and F. K. Larsen, Acta Cryst. A **30**, 580, (1974).

[27] P. Coppens, Crystallographic Computing, in: F. R. Ahmed (Ed.), Munksgaard International Booksellers and Publishers Ltd., Copenhagen, 1979, pp. 255.

[28] J. Rodríguez-Carvajal, Physica B **192**, 55 (1992). Available at https://www.ill.eu/sites/fullprof/

[29] K. Momma and F. Izumi, J. Appl. Cryst. **44**, 1272 (2011).

[30] J.M. Perez-Mato, S.V. Gallego, E.S. Tasci, L. Elcoro, G. de la Flor, and M.I. Aroyo, Annu. Rev. Mater. Res. **45**, 217 (2015).

[31] B. J. Campbell, H. T. Stokes, D. E. Tanner, and D. M. Hatch, "ISODISPLACE: An Internet Tool for Exploring Structural Distortions." J. Appl. Cryst. **39**, 607 (2006); H. T. Stokes, D. M. Hatch, and B. J. Campbell, ISODISTORT, ISOTROPY Software Suite, iso.byu.edu.

[32] N. V. Belov, N. N. Neronova, and T. S. Smirnova, Sov. Phys. Crystallogr. **2**, 311 (1957).

[33] E.F. Bertaut, Acta Crystallogr. Sect. A **24** 2177 (1968).

Compound / T(K)	**$PrBaMn_2O_6$ / 283 K**	
Parent space group	*P4/mmm* (No. 123)	
Propagation vector(s)	(0, 0, 0)	
Transformation from parent basis to the one used	(**a**,**b**,**c**;0,0,0)	
MSG symbol	*P4/mm'm'*	
MSG number	123.345	
Transformation from basis used to standard setting of MSG	(**a**,**b**,**c**;0,0,0)	
Magnetic point group	4/m m' m' (No. 15.6.58)	
Unit cell parameters (Å)	a=3.889(1) α=90º b=3.889(1) β =90º c=7.7317(2) γ =90º	
*MSG symmetry operations	x,y,z,+1 -y,x,z,+1 y,-x,z,+1 -x,-y,z,+1 -x,-y,-z,+1 y,-x,-z,+1 -y,x,-z,+1 x,y,-z,+1 x,-y,-z,-1 -x,y,-z,-1 y,x,-z,-1 -y,-x,-z,-1 -x,y,z,-1 x,-y,z,-1 -y,-x,z,-1 y,x,z,-1	{1|0,0,0} {2_{001}|0,0,0} {4^+_{001}|0,0,0} {4^-_{001}|0,0,0} {$\bar{1}$|0,0,0} {m_{001}|0,0,0} {$\bar{4}^+_{001}$|0,0,0} {$\bar{4}^-_{001}$|0,0,0} {$2'_{100}$|0,0,0} {$2'_{010}$|0,0,0} {$2'_{1\text{-}10}$|0,0,0} {$2'_{110}$|0,0,0} {m'_{100}|0,0,0} {m'_{010}|0,0,0} {$m'_{1\text{-}10}$|0,0,0} {m'_{110}|0,0,0}
Positions of magnetic atoms	Mn ½ ½ 0.2469	
Positions of non-magnetic atoms	Pr 0, 0, 0 Ba 0, 0, ½ O1 ½, ½, 0 O2 ½, 0, 0.2297 O3 0.4934, 0.4934, ½	
Magnetic moments components (μ_B) of magnetic atoms, their symmetry constraints and moment magnitudes.	Mn 0, 0. -1.51(2) (0,0,mz) 1.51(2)	

*Magnetic space group (MSG) symmetry operations obtained from Bilbao Crystallographic Server [29].

Table 1. Description of the magnetic structure for $PrBaMn_2O_6$ at 283 K.

Compound / T(K)	**$PrBaMn_2O_6$ / 12 K**	
Parent space group	*$P2_1am$* (No. 26)	
Propagation vector(s)	(0, 0, 0)	
Transformation from parent basis to the one used	(**a**,**b**,**c**;0,0,0)	
MSG symbol	*$P2_1'a'm$*	
MSG number	26.69	
Transformation from basis used to standard setting of MSG	(-**c**,**b**,**a**;0,0,0)	
Magnetic point group	2_1' m' m (No. 7.3.22)	
Unit cell parameters (Å)	a=5.530(2) α=90º b=5.538(2) β =90º c=7.5815(3) γ =90º	
*MSG symmetry operations	x,y,z,+1 x,y,-z,+1 x+1/2,-y,-z,-1 x+1/2,-y,z,-1	{1|0,0,0} {m_{001}|0,0,0} {$2'_{100}$|1/2,0,0} {m'_{010}|1/2,0,0}
Positions of magnetic atoms	Mn 0.2500, 0.2479, 0.2470	
**Positions of non-magnetic atoms	Pr 0.7316, 02391, 0 Ba 0.7418, 0.2440, ½ O1 0.2396, 0.2246, 0 O2_1 -0.0129, 0.0013, 0.2405 O2_2 -0.0088, 0.4988, 0.2177 O3 0.2396, 0.2680, ½	
Magnetic moments components (μ_B) of magnetic atoms, their symmetry constraints and moment magnitudes.	Mn 3.11(2), 0. 0 (mx,my,mz) 1.51(2)	

*Magnetic space group (MSG) symmetry operations obtained from Bilbao Crystallographic Server [29].** The O2 atom is split into two orbits, O2_1 and O2_2, in the orthorhombic phase.

Table 2. Description of the magnetic structure for $PrBaMn_2O_6$ at 12 K.

FIGURES.

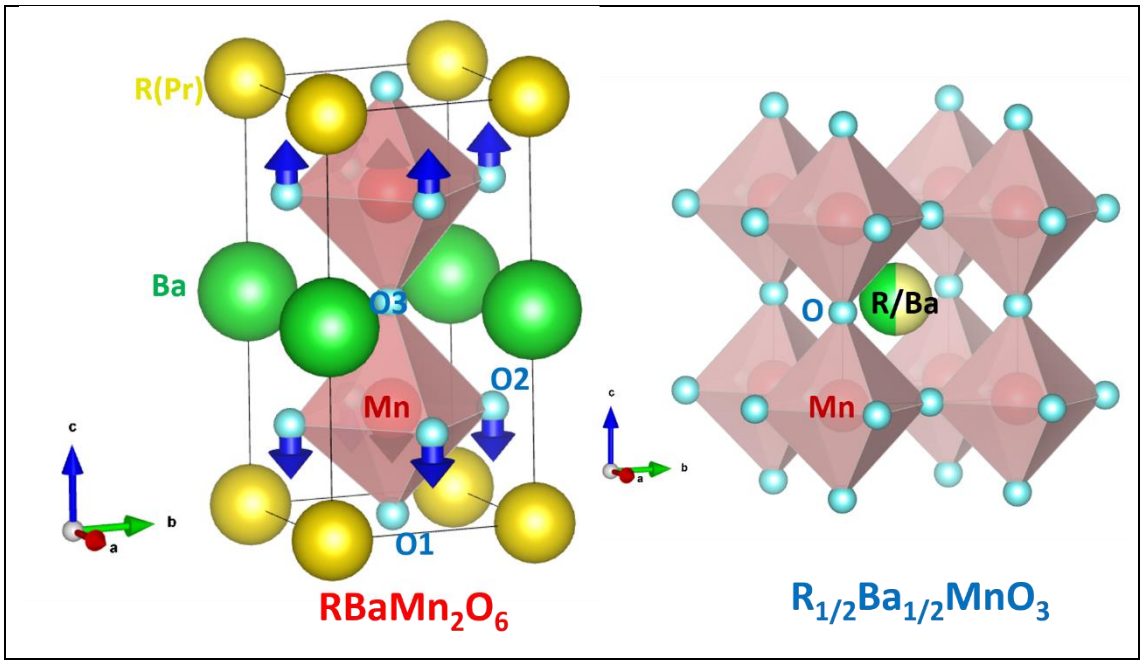

Figure 1. (left) Crystal structure of layered $RBaMn_2O_6$ perovskites with a tetragonal unit cell; (right) crystal structure for disordered $R_{1/2}Ba_{1/2}MnO_3$ compounds with a simple cubic perovskite structure. The arrows show the atomic shifts induced by the size difference between R and Ba atoms.

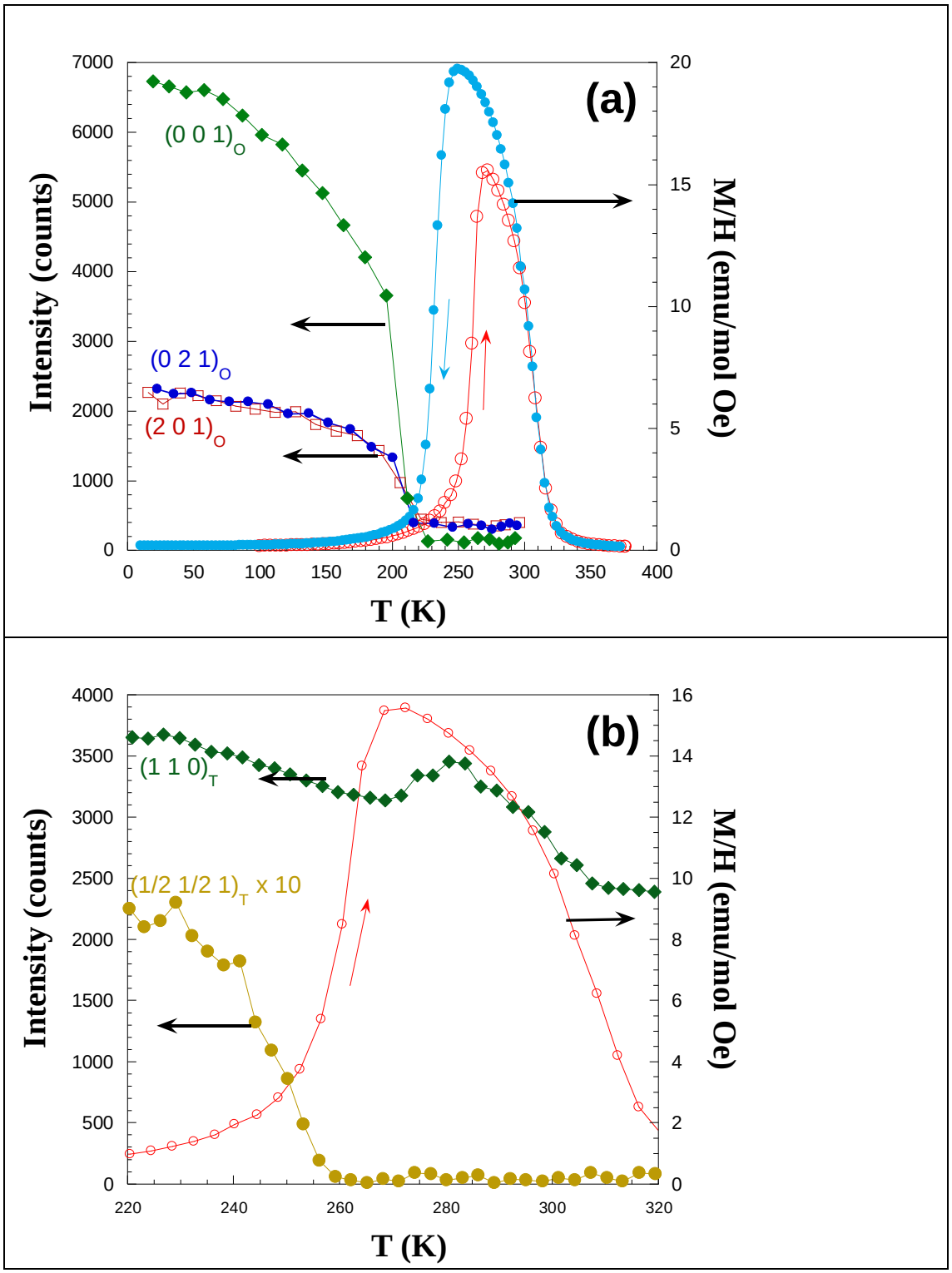

Figure 2. (a) Temperature dependence of the main magnetic reflections (orthorhombic setting) on a cooling ramp compared to the dc magnetization (heating and cooling ramps) for $PrBaMn_2O_6$. (b) Comparison between the temperature dependence of selected reflections (tetragonal setting) and dc magnetization in the heating ramp for the same sample.

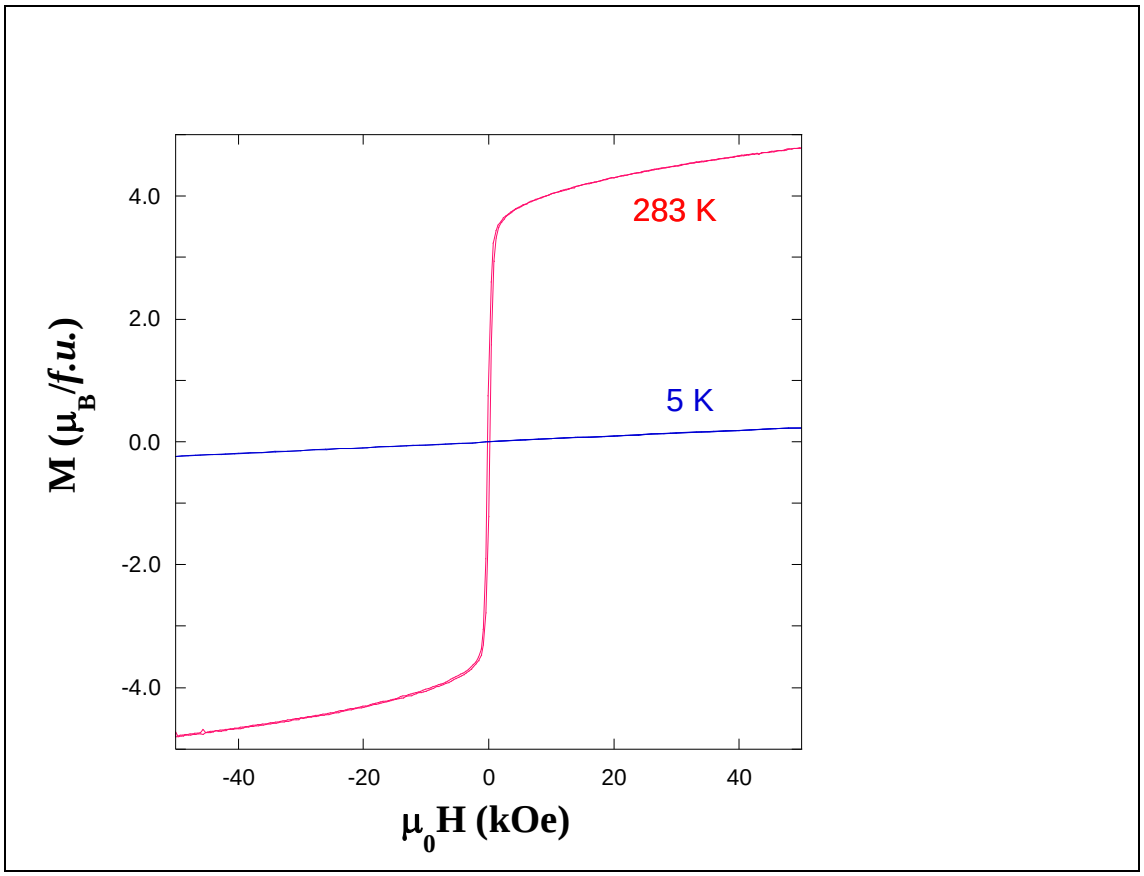

Figure 3. Isothermal magnetization curves for $PrBaMn_2O_6$ measured at 5 and at 283 K.

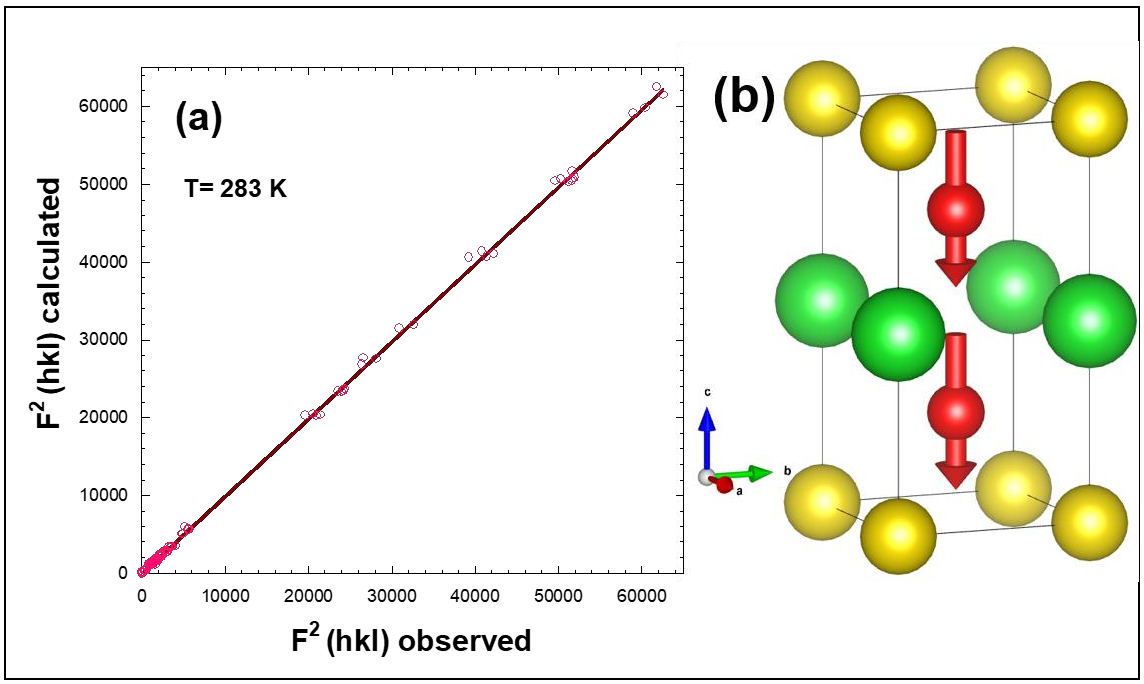

Figure 4. (a) Calculated versus observed squared structure factors for refined single crystal neutron diffraction data collected at 283 K for tetragonal $PrBaMn_2O_6$. 232 reflections were measured and the reliability factors for the fit are R_F= 4.6% and χ^2=1.9. (b) Representation of the tetragonal ferromagnetic structure for $PrBaMn_2O_6$ at 283 K. Oxygens have been omitted for the sake of clarity.

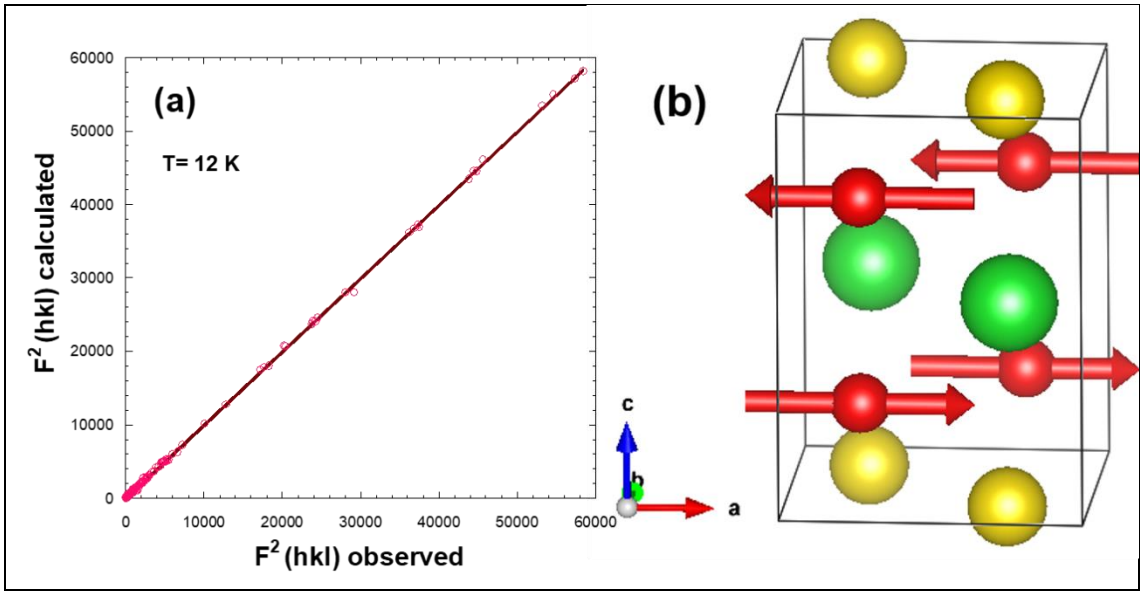

Figure 5. (a) Calculated versus observed values of the squared structure factors for refined single crystal neutron diffraction data collected at 12 K for $PrBaMn_2O_6$. 370 reflections have been measured and the reliability factors for the fit are R_F= 4.3% and χ^2=6.5. (b) Representation of the orthorhombic antiferromagnetic structure for $PrBaMn_2O_6$ at 12 K. Oxygens have been omitted for the sake of clarity.